Available online at www.sciencedirect.com
ScienceDirect
International Journal of Heat and Mass Transfer 51 (2008) 948–959
International Journal of HEAT and MASS TRANSFER
www.elsevier.com/locate/ijhmt

Technical Note

Analysis of a passive vapor feed direct methanol fuel cell

Jeremy Rice, Amir Faghri *

Department of Mechanical Engineering, University of Connecticut, 261 Glenbrook Road, Unit 2237, Storrs, CT 06269, United States

Received 14 July 2007; received in revised form 21 August 2007
Available online 18 October 2007

Abstract

The passive fuel delivery systems presented thus far have utilized the liquid phase as a transport medium. However, since methanol is a highly volatile component, the vapor phase can be utilized to transport methanol to the fuel cell. A one-dimensional analysis of the transport of methanol from the fuel source to the fuel cell is developed here, with the goal of describing the key issues. Operation of the fuel cell is further characterized with a full numerical model that captures transience, and also addresses fuel, water, and thermal management issues. The results show that the condensation of water onto a methanol evaporation pad needs to be limited if the operation time of the fuel cell is to increase.

1. Introduction

The direct methanol fuel cell (DMFC) is being considered as a highly promising candidate for portable power source. The DMFC is an electrochemical reactor that generates electricity based on the methanol oxidation and oxygen reduction with simultaneous mass, charge and energy transfer. The DMFCs have many important advantages over such as quick start-up, longer duration, refueling ability, ambient temperature and pressure operation, and compact cell design.

The passive DMFC systems supply fuel to the anode side in a passive manner without external moving parts. A series of passive liquid feed DMFC prototypes have been developed in recent years. Guo and Faghri [1,2] developed a new miniature DMFC with passive thermal-fluids management system. The system included a fuel cell stack, a fuel tank, and a thermal-fluids system that utilized passive approaches for fuel storage and delivery, air-breathing, water management, CO_2 release and thermal management. A prototype with 5.1 g of neat methanol in the fuel cartridge has successfully demonstrated 18 h of continuous operation with total power output of 1.56 W h.

Guo and Faghri [3,4] also designed planar air-breathing direct methanol fuel cell stacks. The fuel cell incorporated a window-frame structure that provides a large open area for more efficient mass transfer. The membrane electrode assembly and gas diffusion layers are laminated together to reduce contact resistance. The results showed that peak power outputs of 519 mW and 879 mW were achieved in the stacks with active areas 18.0 m and 36 cm^2.

Jewett et al. [5] developed a water management system for a passive DMFC. Water was recovered from the cathode of the cell by adding water management layers to the cathode of the cell, which had a micro-porous layer of 50 wt% PTFE on a carbon cloth. The micro-porous layer increased the hydraulic pressure at the cathode and forced water to pass back through the membrane to the anode. Two water management layers were found to be adequate to maintain a water balance coefficient greater than zero for all current loadings. The air management system used various porous media for air filters to block air-borne particles from reaching the cathode. An oil sorbents filter was found to be the best air filter based on its effects on cell performance, efficiency, and water balance coefficient.

A vapor feed direct methanol fuel cell has potential over a liquid fed system in several ways. It has the potential for shorter start-up times, because the mass diffusivity is several orders of magnitude greater than in the liquid phase.

* Corresponding author. Tel.: +1 860 486 0419; fax: +1 860 486 5088.
E-mail address: amir.faghri@uconn.edu (A. Faghri).

0017-9310/$ - see front matter © 2007 Elsevier Ltd. All rights reserved.
doi:10.1016/j.ijheatmasstransfer.2007.08.025

Nomenclature

A	area of fuel cell (m^2)
$\mathbf{A}$	Stefan–Maxwell flux coefficient matrix (s/m^2)
a	constant in coefficient matrix
a_{ox}	specific area for oxidation (m^{-1})
a_{red}	specific area for reduction (m^{-1})
b	element in solution matrix
$\mathbf{B}$	mole fraction to mass fraction conversion matrix
c_{MeOH}	methanol concentration in liquid (mol/cm^3)
c_{H_2O}	water concentration in liquid (mol/cm^3)
c_p	specific heat (J/kg K)
d_g	characteristic length of gas phase (m)
D_{ij}	binary diffusivity (m^2/s)
$D_{eff,ij}$	effective diffusivity of gas phase (m^2/s)
F	Faraday constant (coulomb/mol)
$\mathbf{g}$	gravity (m/s^2)
h	sensible heat (J/kg)
h^0	heat of formation (J/kg)
h_m	mass transfer coefficient ($kg/s\ m^2$)
$I_{0,ref}^{MeOH}$	oxidation exchange current density (A/m^2)
$I_{0,ref}^{O_2}$	reduction exchange current density (A/m^2)
$\mathbf{I}$	current density (A/m^2)
$\mathbf{I}_p$	proton current density ($proton/m^2\ s$)
$\mathbf{J}$	mass flux ($kg/m^2\ s$)
$J(s)$	leverette function
k	thermal conductivity (W/m K)
k_{rg}	relative permeability of gas phase
k_{rl}	relative permeability of liquid phase
$\mathbf{K}$	permeability (m^{-2})
$\dot{m}'''$	mass source ($kg/m^3\ s$)
$\dot{\mathbf{m}}''$	total species mass flux ($kg/m^2\ s$)
M_i	molecular weight of component i (kg/mol)
M_g	molecular weight of gas (kg/mol)
M_l	molecular weight of liquid (kg/mol)
$\mathbf{n}$	surface normal vector
n_d	electro-osmotic drag coeff. (mol/mol)
Nu	Nusselt number
p_c	capillary pressure (Pa)
p_l	liquid pressure (Pa)
p_g	gas pressure (Pa)
Pr	Prandtl number
R_u	ideal gas constant (J/mol K)
R_Ω	resistance (Ω)
R_{ox}	oxidation reaction rate (A/m^3)
R_{red}	reduction reaction rate (A/m^3)
Re_ε	pore Reynolds number
t	time (s)
T	temperature (K)
s	liquid saturation
Sh	Sherwood number
$\mathbf{V}$	local velocity (m/s)
$\langle \mathbf{V}_k \rangle^k$	intrinsic phase velocity of phase k (m/s)
V	volume (m^3)
x_{MeOH}	mole fraction of methanol in liquid (mol/mol)
x	distance in x-direction (m)
y	distance in y-direction (m)
α_l	liquid volume fraction
$\alpha_{l,MeOH}$	volume fraction of MeOH in liquid phase
α_a	anode transfer coefficient
α_c	cathode transfer coefficient
β	equilibrium constant in condensible phases
ε	porosity
ϕ	electric potential (V)
η	usage ratio
η_a	anodic overpotential (V)
η_c	cathodic overpotential (V)
λ	oxidation constant (mol/cm^3)
μ	viscosity ($N\ s/m^2$)
Ψ	non-dimensional total mass flux
ψ_i	non-dimensional species mass flux
θ	contact angle between liquid and solid (rad)
σ	surface tension (N/m)
σ_c	electrical conductivity of carbon phase ($\Omega^{-1}\ m^{-1}$)
σ_m	proton conductivity of membrane phase ($\Omega^{-1}\ m^{-1}$)
ρ	density (kg/m^3)
τ	tortuosity
$\omega_{g,i}$	mass fraction of gas (kg/kg)
$\omega_{l,i}$	mass fraction of liquid (kg/kg)
ζ	stoichiometric coefficient

Subscripts

acl	anode catalyst layer
agdl	anode gas diffusion layer
ccl	cathode catalyst layer
cgdl	cathode gas diffusion layer
e	entrance
g	gas
i	component i
j	component j
l	liquid
m	membrane
n	neighboring cells
ref	reference/ambient conditions
R	due to chemical reaction
T	due to mass transport (evaporation/condensation)

Superscripts

k	previous iteration
$k+1$	next iteration

It also has the potential to have a higher operating temperature, thus increasing the reaction rates, resulting in higher power outputs. However, at a higher operating temperature, water management becomes a key issue because the evaporative losses are much greater. Also, for a compact system, the methanol will need to be stored in its liquid state. Since methanol is a very volatile substance, it can easily be evaporated and delivered to the fuel cell through the vapor phase.

Guo and Faghri [6,7] later expanded the capillary concepts for the liquid feed DMFC systems to make a new innovative vapor feed system. They developed a semi-passive vapor feed direct methanol fuel cell. The semi-passive description is used because a heat source is needed for the fuel cell to run for long periods of time since water condensation on a methanol evaporation pad can limit the operating time. Pure methanol was wicked from a reservoir to an evaporation pad where heat is applied and methanol was vaporized. The heat can come from a variety of sources such as, electrical heating, catalyst burning and heat recovery from the cell or the device it is powering. The delivery system showed long-term stability for over 600 h using a catalytic burner.

Kim et al. [8,9] developed a semi-passive DMFC which is fueled by methanol vapor. Methanol is fed into porous foam by a syringe pump. Methanol is vaporized through a layer of Nafion 112 and then diffuses through a water barrier layer and a buffer layer. The vapor feed system was able to run for 360 h between 20 and 25 mW/cm^2. The fuel efficiency was 70% higher than the liquid fuel efficiency, and the energy density was 1.5 times greater than liquid energy density.

Fukunaga et al. [10] measured anode performance and impedance spectra with different catalyst and ionomer loading to clarify the characteristics of vapor feed DMFCs. The impedance spectra were deconvolved into three semicircles with different time constants, each showing a different dependence on the anodic polarization. The middle-frequency range arc decreased as the anodic polarization increased, indicating that this process represents the oxidation reaction of methanol. The high-frequency range arc showed little dependence on the anodic polarization, but increased with the thickness of the electrode, indicating that this process might be related to proton conduction through the electrode. The low-frequency range arc was observed only when the methanol concentration was low, in contrast to liquid feed DMFCs (LF-DMFCs), for which the removal of the product gas presents a large resistance. A simpler design can therefore be used for a VF-DMFC, giving it an advantage over an LF-DMFC. A decreasing ionomer to catalyst ratio (I/C) caused the interfacial conductivity (σE) to increase, but it intensively decreased when I/C was below 0.25.

Shukla et al. [11] presented on a vapor feed direct-methanol fuel cell employing a proton-exchange membrane electrolyte. The fuel cell could be operated with 1% methanol, giving a typical performance of 550 mV at 75 mA cm^{-2}, and a fuel utilization coefficient of 0.56. At 2 M methanol concentration, the cell voltage load found to be 610–550 mV at a load current density of 100 mA cm^{-2}. The observed open-circuit potentials of this cell assembly have been found to be in the range 850–980 mV.

Hogarth et al. [12] described the construction of a gas-fuel feed direct methanol fuel cell and reviewed the optimization of the active electrode fabrication process. For this vapor phase-system, it has proved possible to develop a Nafion encapsulated process in which the porous carbon electrodes were bonded with Nafion rather than PTFE. Initially, PTFE was removed only from the anode paste, but it was found that PTFE was also unnecessary at the cathode. The best performance was found for extremely thin catalysed carbon layers at the two electrodes, and to reduce loadings, thin layers of uncatalysed carbon were inserted between the carbon cloth current collectors and the catalysed carbon layers. The final electrodes had loadings of 2 mg/cm^2 on the anode and 0.5 mg/cm^2 on the cathode and gave peak power densities of 0.35 W/cm^2 with oxygen and 0.22 W/cm^2 with air as the combustant.

In order to understand transport and electrochemical phenomena and optimize cell design and operation conditions, some mathematical models for vapor feed DMFCs have been developed in recent years. Scott et al. [13] reported the performance and modeling of vapor feed DMFCs. Two sizes of cell are used: a small cell with an area of 9 cm^2 and a large single cell with an area of 250 cm^2. The methanol crossover from the anode to the cathode through the polymer membrane was considered in their model. The mathematical model also described mass transport in the porous electrode structures and the potential and concentration distributions in the electrode regions. The cell voltage and current density response of the fuel cell were predicted. Dohle et al. [14] presented an isothermal, steady-state, one-dimensional model for the vapor feed DMFC including the crossover phenomenon. The numerical calculation is based on the finite integration technique and was performed on the mathematical and physicochemical basis of an earlier-developed PEMFC model. The effects of methanol concentration on the cell performance were studied. Kulikovsky et al. [15] presented a two-dimensional macro-homogeneous model to describe the reaction and transport for a vapor feed DMFC with new current collectors. The model employed Stefan–Maxwell molecular diffusion in the gas diffusion layers and the Knudsen diffusion mechanism in the catalyst layers, but neglected the methanol crossover and the influence of the normal gradients in the flow channel. More models and technical challenges in fuel cells were reviewed by Refs. [16,17].

The fundamentals of a vapor feed DMFC in passive operation are considered with the one-dimensional mass transport of methanol vapor, water vapor, and carbon dioxide. This analysis is useful in dimensioning the vapor

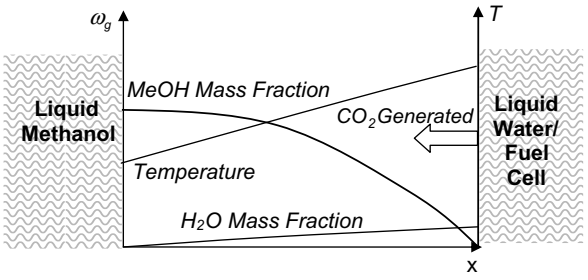

Fig. 1. Schematic of mass transport process for a vapor feed DMFC through a gaseous medium between a pure methanol source and the fuel cell.

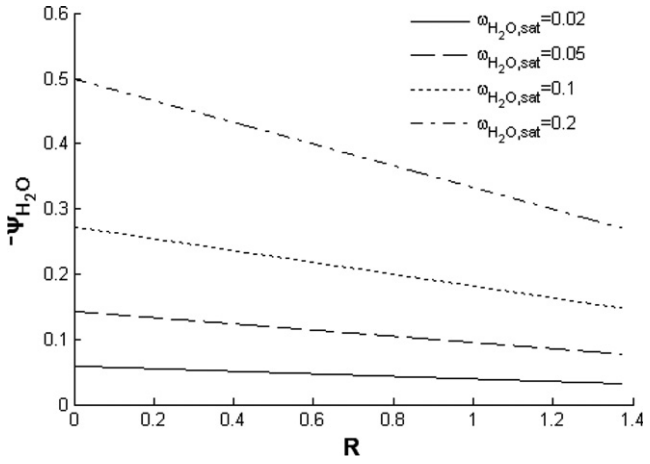

Fig. 2. Normalized condensation rate of water into the methanol solution versus the relative CO_2 flow rate in the diffusion region with the methanol solution held at 25 °C.

diffusion region between a pure methanol source and the fuel cell as well as understanding the mass transport of water vapor to the pure methanol fuel. The results of this analysis are used to describe the long-term operation of a passively feed system. In addition to the one-dimensional analysis, a multiphase flow model considered the entire system, including energy effects. The results from the model describe start-up effects, water management, and thermal management issues associated with a vapor fed system.

2. Passive vapor feed fundamentals

Methanol can be fed to the fuel cell through the vapor phase by passive means. The major transport phenomenon governing this process is methanol evaporating from a nearly pure liquid methanol source in a porous media and condensing into a highly dilute methanol solution at the anode side of a fuel cell. The reverse transport of water vapor also occurs, however this process is much slower because water has a much lower vapor pressure than methanol at a given temperature. Also, carbon dioxide is generated in the oxidation reaction, and must leave the fuel cell from the anode gas diffusion layer. A schematic of this process is presented in Fig. 1. The mass transport for a particular component is governed by

$$\rho \mathbf{V} \omega_i - \rho D \frac{\mathrm{d}\omega_i}{\mathrm{d}x} = \dot{\mathbf{m}}_i'' \tag{1}$$

The total mass flux, is simply a summation of all the species fluxes.

$$\rho \mathbf{V} = \sum_i \dot{\mathbf{m}}_i'' \tag{2}$$

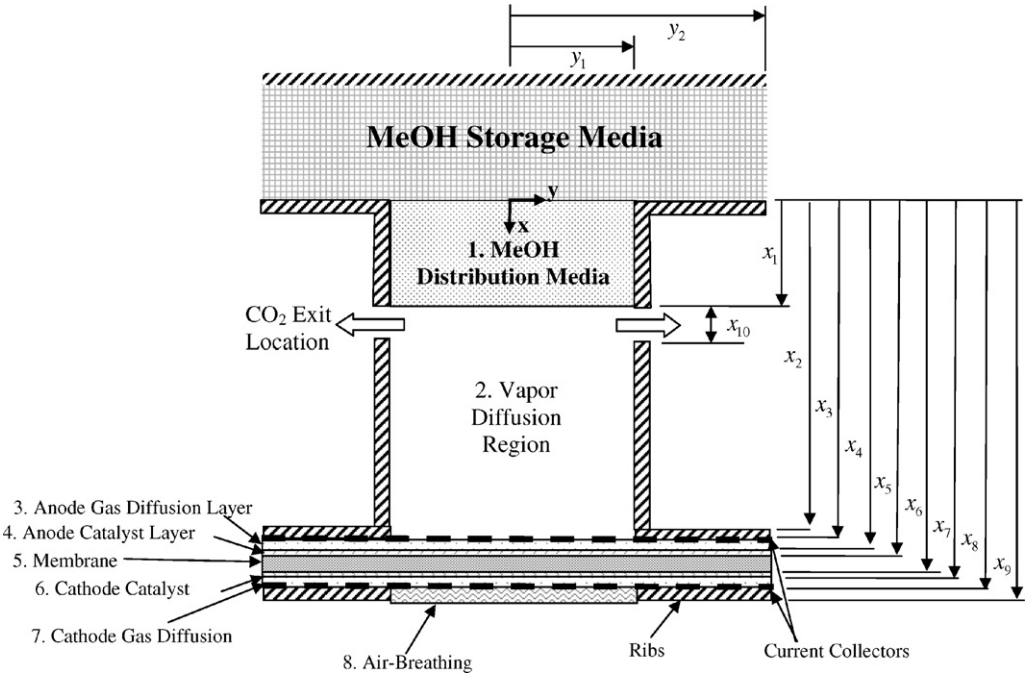

Fig. 3. Schematic of a passive vapor feed DMFC.

Table 1
Governing equations

Continuity		
Liquid	$\frac{\partial}{\partial t}(\varepsilon s\rho_{\mathrm{l}}) + \nabla\cdot(\varepsilon s\rho_{\mathrm{l}}\langle\mathbf{V}_{\mathrm{l}}\rangle^{\mathrm{l}}) = \dot{m}'''_{\mathrm{l}}$	(15)
Gas	$\frac{\partial}{\partial t}(\varepsilon(1-s)\rho_{\mathrm{g}}) + \nabla\cdot\left(\varepsilon(1-s)\rho_{\mathrm{g}}\langle\mathbf{V}_{\mathrm{g}}\rangle^{\mathrm{g}}\right) = \dot{m}'''_{\mathrm{g}}$	(16)
Momentum		
Liquid	$\varepsilon s\langle\mathbf{V}_{\mathrm{l}}\rangle^{\mathrm{l}} = -\frac{k_{\mathrm{rl}}\mathbf{K}}{\mu_{\mathrm{l}}}\nabla p_{\mathrm{l}} + \frac{n_{\mathrm{d}}M_{\mathrm{l}}}{\rho_{\mathrm{l}}}\frac{\mathbf{I}_{\mathrm{p}}}{F} \quad s > s_{ir,\mathrm{l}}$ $\varepsilon s\langle\mathbf{V}_{\mathrm{l}}\rangle^{\mathrm{l}} = 0 \quad s \leqslant s_{ir,\mathrm{l}}$	(17)
Gas	$\varepsilon(1-s)\langle\mathbf{V}_{\mathrm{g}}\rangle^{\mathrm{g}} = -\frac{k_{\mathrm{rg}}\mathbf{K}}{\mu_{\mathrm{g}}}\nabla p_{\mathrm{g}} \quad s < s_{ir,\mathrm{g}}$ $\varepsilon(1-s)\langle\mathbf{V}_{\mathrm{g}}\rangle^{\mathrm{g}} = 0 \quad s \geqslant s_{ir,\mathrm{g}}$	(18)
Species		
Liquid	$\frac{\partial}{\partial t}(\varepsilon s\rho_{\mathrm{l}}\omega_{\mathrm{l},i}) + \nabla\cdot\left(\dot{\mathbf{m}}''_{\mathrm{l},i}\right) = \dot{m}'''_{\mathrm{l},i}$	(19)
	$\dot{\mathbf{m}}''_{\mathrm{l},i} = \varepsilon s\rho_{\mathrm{l}}\langle\mathbf{V}_{l}\rangle^{\mathrm{l}}\omega_{\mathrm{l},i} - [\varepsilon s]^{\tau}\rho_{l}D_{\mathrm{l},12}\nabla\omega_{\mathrm{l},i} \quad s > s_{ir,\mathrm{l}}$ $\dot{\mathbf{m}}''_{\mathrm{l},i} = 0 \quad s \leqslant s_{ir,\mathrm{l}}$	(20)
Gas	$\frac{\partial}{\partial t}(\varepsilon(1-s)\rho_{\mathrm{g}}\omega_{\mathrm{g},i}) + \nabla\cdot\left(\dot{\mathbf{m}}''_{\mathrm{g},i}\right) = \dot{m}'''_{\mathrm{g},i}$	(21)
	$\dot{\mathbf{m}}''_{\mathrm{g},i} = \varepsilon(1-s)\rho_{\mathrm{g}}\langle\mathbf{V}_{\mathrm{g}}\rangle^{\mathrm{g}}\omega_{\mathrm{g},i} - \sum_{j=1}^{N-1}[\varepsilon(1-s)]^{\tau}\rho_{\mathrm{g}}D_{\mathrm{eff},ij}\nabla\omega_{\mathrm{g},j} \quad s < s_{ir,\mathrm{g}}$ $\dot{\mathbf{m}}''_{\mathrm{g},i} = 0 \quad s \geqslant s_{ir,\mathrm{g}}$	(22)
Energy		
Mixture	$\frac{\partial}{\partial t}\left(\varepsilon s\rho_{\mathrm{l}}\bar{h}_{\mathrm{l}} + \varepsilon(1-s)\rho_{\mathrm{g}}\bar{h}_{\mathrm{g}} + (1-\varepsilon)\bar{h}_{\mathrm{s}}\right) + \sum_i\nabla\cdot\left(\dot{\mathbf{m}}''_{\mathrm{l},i}\bar{h}_{\mathrm{l},i} + \dot{\mathbf{m}}''_{\mathrm{g},i}\bar{h}_{\mathrm{g},i}\right)$ $= \nabla\cdot(k_{\mathrm{eff}}\nabla T) - \sum_i\dot{m}'''_{\mathrm{l},i}h^{0}_{\mathrm{l},i} - \sum_i\dot{m}'''_{\mathrm{g},i}h^{0}_{\mathrm{g},i} + \nabla\cdot(\phi_{\mathrm{m}}\sigma_{\mathrm{m}}\nabla\phi_{\mathrm{m}}) + \nabla\cdot(\phi_{\mathrm{c}}\sigma_{\mathrm{c}}\nabla\phi_{\mathrm{c}})$	(23)
Electric potential		
Carbon phase	$\nabla\cdot(\sigma_{\mathrm{c}}\nabla\phi_{\mathrm{c}}) - R_{\mathrm{ox}} + R_{\mathrm{red}} = 0$	(24)
Membrane phase	$\nabla\cdot(\sigma_{\mathrm{m}}\nabla\phi_{\mathrm{m}}) + R_{\mathrm{ox}} - R_{\mathrm{red}} = 0$	(25)

Since the water and methanol vapor mass fractions range from their saturation value to approximately zero, the mass fraction is normalized to be between zero and unity.

$$\bar{\omega}_i = \frac{\omega_i}{\omega_{i,\mathrm{sat}}} \tag{3}$$

Also, the length between the pure methanol solution and the fuel cell is also normalized. Finally, the total equation is normalized by the mass flux of methanol needed to apply a particular current density. Therefore, the following non-dimensional numbers appear.

Table 2
Closure relations and secondary conditions

Interphase momentum relations

Capillary pressure

$$p_c = p_g - p_l = \sigma\cos\theta\left(\frac{\varepsilon}{K}\right)^{1/2} J(s) \tag{26}$$

$$J(s) = \begin{cases} 1.417(1-s) - 2.120(1-s)^2 + 1.263(1-s)^3 & \theta < \pi/2.0 \\ 1.417s - 2.120s^2 + 1.263s^3 & \theta \geqslant \pi/2.0 \end{cases} \tag{27}$$

Relative permeability

$$k_{rl} = s^3 \tag{28}$$

$$k_{rg} = (1 - s)^3 \tag{29}$$

Species equilibrium conditions

MeOH and H_2O

$$\omega_{g,i} = \beta_i \omega_{l,i}$$
$$\beta_i = \frac{M_l p_{ref}}{M_g p_{op}} \exp\left(\frac{h_{fg} M_i}{R}\left(\frac{1}{T_{ref}} - \frac{1}{T}\right)\right) \tag{30}$$

Specises diffusion

Stefan–Maxwell in gas

$$[D_{eff}, ij] = \mathbf{A}^{-1}\mathbf{B} \tag{31}$$

$$A_{ii} = -\frac{\omega_{g,i} M_g^2}{D_{iN} M_N M_i} - \sum_{\substack{k=1 \\ k\neq i}}^{N} \frac{\omega_{g,k} M_g^2}{D_{ik} M_k M_i}; \quad A_{ij} = \omega_{g,i}\frac{M_g^2}{M_i}\left(\frac{1}{D_{ij} M_j} - \frac{1}{D_{iN} M_N}\right), \quad i \neq j \tag{32}$$

$$B_{ii} = -\frac{M_g}{M_i}\left(1 - \frac{M_g \omega_{g,i}}{M_i}\right) - \frac{M_g^2 \omega_{g,i}}{M_i M_N}; \quad B_{ij} = \frac{M_g^2 \omega_{g,i}}{M_i}\left(\frac{1}{M_j} - \frac{1}{M_N}\right), \quad i \neq j \tag{33}$$

Energy transport

Liquid

$$h_{l,i} = \int_{T_{ref}}^{T} c_{p_{l,i}} \mathrm{d}T + h_{l,i}^0 = \bar{h}_{l,i} + h_{l,i}^0$$
$$\bar{h}_l = \sum_i \omega_{l,i} \bar{h}_{l,i} \tag{34}$$

Gas

$$h_{g,i} = \int_{T_{ref}}^{T} c_{p_{g,i}} \mathrm{d}T + h_{g,i}^0 = \bar{h}_{g,i} + h_{g,i}^0$$
$$\bar{h}_g = \sum_i \omega_{g,i} \bar{h}_{g,i} \tag{35}$$

Thermal conductivity

$$k_{eff} = \varepsilon s k_l + \varepsilon(1-s)k_g + (1-\varepsilon)k_s \tag{36}$$

$$\bar{x} = \frac{x}{L}, \quad \Psi = \frac{6F\rho\mathbf{V}}{M_{MeOH}\mathbf{I}}, \quad \psi_i = \frac{6F\dot{\mathbf{m}}_i''}{M_{MeOH}\mathbf{I}},$$
$$Pe = \frac{M_{MeOH}\mathbf{I}L}{6F\rho D} \tag{4}$$

The governing equations for methanol and water vapor can be rewritten in terms of these non-dimensional parameters.

$$\Psi\bar{\omega}_i - \frac{1}{Pe}\frac{\mathrm{d}\bar{\omega}}{\mathrm{d}\bar{x}} = \frac{\psi_i}{\omega_{i,sat}} \tag{5}$$

The total mass flux is now:

$$\Psi = \sum_i \psi_i \tag{6}$$

Identically, the methanol mass flux is set to unity in the ideal case of no methanol cross-over. Also, depending on

Table 3
Initial and boundary conditions

Initial conditions		
Liquid phase saturation	$s = s_0 \quad x < x_1 \quad \text{and} \quad x_4 \leqslant x \leqslant x_7$ $s = 0 \quad x_1 \leqslant x < x_4 \quad \text{and} \quad x > x_7$	(37)
Species mass fractions Methanol and water	$\omega_{\text{l,MeOH}} = 1 \qquad x < x_1$ $\omega_{\text{l,MeOH}} = 0 \quad x \geqslant x_1$	(38)
	$\omega_{\text{g},i} = \omega_{\text{g},i,\text{sat}} \quad s > 0$ $\omega_{\text{g},i} = \omega_{\text{g},i,\text{ref}} \quad s = 0$	(39)
Other components	$\omega_{\text{g,CO}_2} = 1 - \omega_{\text{g,MeOH}} - \omega_{\text{g,H}_2\text{O}}, \omega_{\text{g,O}_2} = \omega_{\text{g,N}_2} = 0 \quad s > 0$ $\omega_{\text{g},i} = \omega_{\text{g},i,\infty} \quad s = 0$	(40)
Energy	$T = T_{\text{ref}}$	(41)
Boundary conditions At symmetry ($y = 0$), top of domain, ($y = y_1, x < x_1, x_1 + x_{10} < x < x_2$), ($y = y_2$)		
	$\nabla \Phi \cdot \mathbf{n} = 0, \quad \Phi = p_l, p_g, \omega_l, i, \omega_g, i, T, \phi_c, \phi_m$	(42)
At CO_2 exit ($y = y_1, x_1 < x \leqslant x_1 + x_{10}$)		
	$\nabla \Phi \cdot \mathbf{n} = 0, \quad \Phi = p_{\text{l}}, \omega_{\text{l},i}, \omega_{\text{g},i}, T$ $p_{\text{g}} = 0$	(43)
At entrance of MeOH distribution media ($x = 0$)		
	$\nabla \Phi \cdot \mathbf{n} = 0, \Phi = p_{\text{g}}, \omega_{\text{l},i}, \omega_{\text{g},i}, T$ $p_{\text{l}} = 0$ $\omega_{\text{l,MeOH}} = 1$	(44)
At surface of air-breathing layer ($x = x_9$)		
	$p_{\text{g}} = 0$ $\langle \mathbf{V}_{\text{l}} \rangle^{\text{l}} \cdot \mathbf{n} = 0$ $-[\varepsilon(1-s)]^{\tau} \nabla \omega_{\text{g},i} \cdot \mathbf{n} = h_{\text{m}}(\omega_{\text{g},i} - \omega_{\text{g},i,\infty})$ $-k_{\text{eff}} \nabla T \cdot \mathbf{n} = h(T - T_{\text{ref}}) + \sigma_{\text{SB}}(T^4 - T_{\text{ref}}^4)$	(45)
Electric potential boundary conditions		
	$x = x_3 \quad \phi_c = 0$ $x = x_4, \ x = x_7 \quad \nabla \phi_m \cdot \mathbf{n} = 0$ $x = x_5, \ x = x_6 \quad \nabla \phi_{\text{c}} \cdot \mathbf{n} = 0$ $x = x_8 \quad \phi_{\text{c}} = V_{\text{cell}}$	(46)

where the carbon dioxide is allowed to leave the vapor diffusion medium, the carbon dioxide mass flux is

$$\psi_{\text{CO}_2} = -R, \quad 0 \leqslant R \leqslant \frac{M_{\text{CO}_2}}{M_{\text{MeOH}}} \tag{7}$$

A value of R equivalent to zero, means that all the carbon dioxide leaves the system right next to the anode gas diffusion layer. The maximum R value means that all the carbon dioxide leaves the system near the pure methanol solution. Therefore, the total mass flux in the vapor region depends on where the carbon dioxide exits.

$$\Psi = 1 - R + \psi_{\text{H}_2\text{O}} \tag{8}$$

Assuming nearly pure methanol exists in the methanol distribution media, and nearly pure water exists in the fuel cell, the boundary conditions for this problem is

$$\begin{aligned} &\bar{x} = 0, \quad \bar{\omega}_{\text{MeOH}} = 1, \quad \bar{\omega}_{\text{H}_2\text{O}} = 0 \\ &\bar{x} = 1, \quad \bar{\omega}_{\text{MeOH}} = 0, \quad \bar{\omega}_{\text{H}_2\text{O}} = 1 \end{aligned} \tag{9}$$

The solutions for the methanol and water mass fractions, after applying the boundary conditions at $\bar{x} = 0$, are:

$$\bar{\omega}_{\mathrm{MeOH}} = (1 + (\omega_{\mathrm{MeOH,sat}}\Psi)^{-1})\exp(\Psi Pe\bar{x}) - (\bar{\omega}_{\mathrm{MeOH,sat}}\Psi)^{-1}$$
$$\bar{\omega}_{\mathrm{H_2O}} = \frac{\psi_{\mathrm{H_2O}}}{\omega_{\mathrm{H_2O,sat}}\Psi}\exp(\Psi Pe\bar{x}) - \frac{\psi_{\mathrm{H_2O}}}{\omega_{\mathrm{H_2O,sat}}\Psi} \tag{10}$$

From the boundary conditions at $\bar{x} = 1$, the following relation can be made:

$$\exp(\Psi Pe) = \frac{\omega_{\mathrm{H_2O,sat}}\Psi}{\psi_{\mathrm{H_2O}}} + 1 = \frac{1}{\omega_{\mathrm{MeOH,sat}}\Psi + 1} \tag{11}$$

Using Eq. (8), the total mass flux is

$$\Psi = \frac{\omega_{\mathrm{MeOH,sat}}(1-R) - \omega_{\mathrm{H_2O,sat}}}{(\omega_{\mathrm{H_2O,sat}} + 1)\omega_{\mathrm{MeOH,sat}}} \tag{12}$$

Therefore, the total mass flux of water is

$$\psi_{\mathrm{H_2O}} = \frac{\omega_{\mathrm{MeOH,sat}}(1-R) - \omega_{\mathrm{H_2O,sat}}}{(\omega_{\mathrm{H_2\ O,sat}} + 1)\omega_{\mathrm{MeOH,sat}}} - 1 + R \tag{13}$$

For the possible values of R, the mass flux of the water is always negative, therefore, water will always condense on the pure methanol solution, which can reduce the mass flux of methanol to the fuel cell. The relative condensation rate of water vapor in the methanol solution is presented in Fig. 2. The methanol saturation mass fraction is held constant resembling a constant temperature, however the water saturation mass fraction is allowed to increase, representing the fuel cell heating up. The water condensation rate can be decreased if the carbon dioxide is forced to leave from near the methanol solution. However, the higher the fuel cell temperature, the higher the condensation rate of water in the methanol solution. It can also be noted that as the methanol saturation mass fraction is increased, the condensation of water decreases. The length of the gas diffusion region can be determined is related to the Peclet number.

$$Pe = \Psi^{-1}\ln\left(\frac{1}{\omega_{\mathrm{MeOH,sat}}\Psi + 1}\right) \tag{14}$$

For a 0.1 A/cm^2 load, the length of the diffusion medium is on the order of centimeters, where as for the liquid delivery system, the length scale is on the order of millimeters.

3. Mathematical modeling

The general schematic of the vapor feed direct methanol fuel cell is presented in Fig. 3. Based on the one-dimensional analysis, the carbon dioxide is allowed to leave near the methanol distribution layer, so as to limit the amount of water condensation in this region. The volume averaged formulation from Rice and Faghri [18,19] is utilized. A summary of the governing equations and the secondary conditions are provided in Tables 1 and 2, respectively. The governing equations are used to solve the thermal and species transport in regions 1–8. The initial and boundary conditions are listed in Table 3. The heat and mass transfer coefficients at the surface of the air-breathing layer are taken from natural convection correlations in Faghri and Zhang [20].

$$Nu = 0.27(GrPr)^{.025}; \quad Nu = \frac{hL}{k}$$
$$Sh = 0.27(GrSc)^{.025}; \quad Sh = \frac{h_{\mathrm{m}}L}{\rho D_{ij}} \tag{47}$$

4. Results

The methanol distribution layer and fuel cell were all identical to the liquid-feed system previously modelled by Rice and Faghri [19]. However, the vapor diffusion region, which is analogous to the water storage media in the liquid-feed system, is an order of magnitude greater in length and contains no liquid. The fuel cell start-up for varying vapor diffusion regions lengths is presented in Fig. 4. The shorter the vapor diffusion length, the faster the cell power density increases and the faster a stable power density is reached. Also the power density is greater with the shorter vapor diffusion length because more methanol is delivered to the fuel cell. The modeling parameters used are listed in Table 4.

The temperature rise of the cathode catalyst layer and the surface of the methanol distribution layer during start-up is presented in Fig. 5. Similarly to the cell power, the temperature of the fuel cell increases to a higher temperature for a shorter vapor diffusion length because the methanol concentration in the fuel cell is increased. In addition to there being more useful cell current, there is also more methanol cross-over, which both produce heat, thus increasing the cell temperature. The temperature of the methanol distribution layer initially drops because of methanol evaporation. For the shorter length scales, the

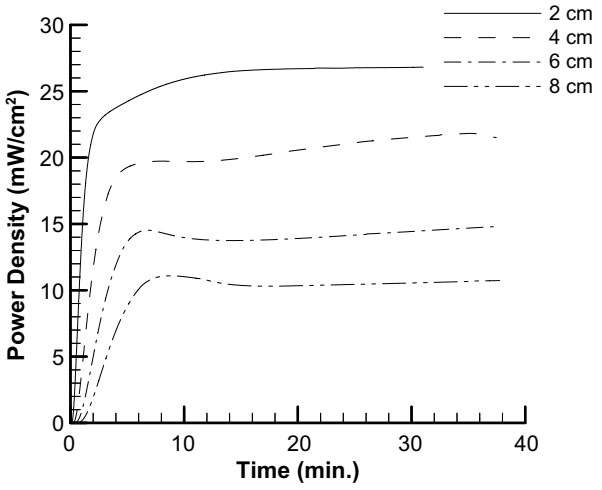

Fig. 4. Cell start-up power output for varying vapor diffusion lengths.

Table 4
Physicochemical properties

Parameter		Value	Ref.
	$K/\varepsilon/\tau$ (m^2/unitless/unitless)	θ, H_2O/MeOH (radians)	
MeOH Distribution	2.5e−13/0.3/1	$1.33\pi/0$	Assumed
H_2O Storage	1e−10/0.9/1	0/0	Assumed
agdl	1e-11/0.7/1	0/0	Assumed
acl	2.5e-12/0.6/1.8	0/0	Assumed
mem.	1e-13/0.5/1.8	0/0	Assumed
ccl	2.5e-11/0.6/1.8	$\frac{\pi}{3}/0$	Assumed
cgdl	1e−10/0.7/1	$1.33\pi/1.33\pi$	Assumed
Diffusivity, gas phase, $D_{ij} = D_{ji}$, (m^2/s),	O_2/CO_2	$0.159 \cdot 10^{-4}$ at 293K, 101.325kPa	Lide [21] for proportionality of form $D_{ij} \propto p^{-1}T^{3/2}$
	O_2/H_2O	$0.244 \cdot 10^{-4}$	
	O_2/N_2	$0.202 \cdot 10^{-4}$	
	CO_2/H_2O	$0.162 \cdot 10^{-4}$	
	CO_2/N_2	$0.160 \cdot 10^{-4}$	
	H_2O/N_2	$0.242 \cdot 10^{-4}$	
	O_2/MeOH, CO_2/MeOH, H_2O/MeOH, MeOH/N_2	Assumed $\left(-0.06954 + 4.5986 \cdot 10^{-4}T + 9.4979 \cdot 10^{-7}T^2\right) \cdot 10^{-4}$	Yaws [22]
Diffusivity, liquid phase,(m^2/s)	MeOH/H_2O	$10^{(-5.4163-999.778/T)}$	Yaws [23]
Density, $\rho_{l,i}$, (kg/m^3)	H_2O	$\exp\left(\begin{array}{l}6.9094 - 2.0146 \cdot 10^{-5}(T-273) - \\ 5.9868 \cdot 10^{-6}(T-273)^2 + 2.5921 \cdot 10^{-8}(T-273)^3 - \\ 9.3244 \cdot 10^{-11}(T-273)^4 + 1.2103 \cdot 10^{-13}(T-273)^5\end{array}\right)$	Faghri [24]
	MeOH	$244.4 \times 0.224^{\left(-\left(1-\frac{T}{513}\right)^{\frac{2}{9}}\right)}$	Yaws [23]
Electro-osmotic drag coefficient, (mol/mol)	n_d	2.5	Ren et al. [25]
Electric Conductivity, (Ω^{-1} m^{-1})	σ_c	4000	Kulikovsky et al. [15]
	σ_m	3.4	
Transfer coefficient	α_a	0.82	Fit to data
	α_c	0.76	
Specific area, (m^{-1})	a_{ox}	17.8	Fit to data
	a_{red}	43478	Assumed
Exchange current	$I_{0,ref}^{MeOH}$	94.25 exp $(35570/R(1/353 - 1/T))$	Wang and Wang [26]
Density, (A/m^2)	$I_{0,ref}^{O_2}$	$0.04222 \exp(732000/R(1/353 - 1/T))$	
Oxidation constant, (mol/cm^3)	λ	4.4×10^{-9}	Fit to data
Reduction reference mass fraction (kg/kg)	$m_{O_2,ref}$	0.23	Wang and Wang [26]
Thermodynamic potential, (V)	U^{MeOH}	−0.0229	Meyers and Newman [27]
	U^{O_2}	1.24	Wang and Wang [26]
Distance, (m)	x_1	$1 \cdot 10^{-2}$	
	$x_3 - x_1$	vary	
	$x_4 - x_3$	$1.5 \cdot 10^{-4}$	
	$x_5 - x_4$	$2.3 \cdot 10^{-5}$	
	$x_6 - x_5$	$1.8 \cdot 10^{-4}$	
	$x_7 - x_6$	$2.3 \cdot 10^{-5}$	
	$x_8 - x_7$	$1.5 \cdot 10^{-4}$	
	y_1	$3.25 \cdot 10^{-3}$	
	y_2	$5 \cdot 10^{-3}$	

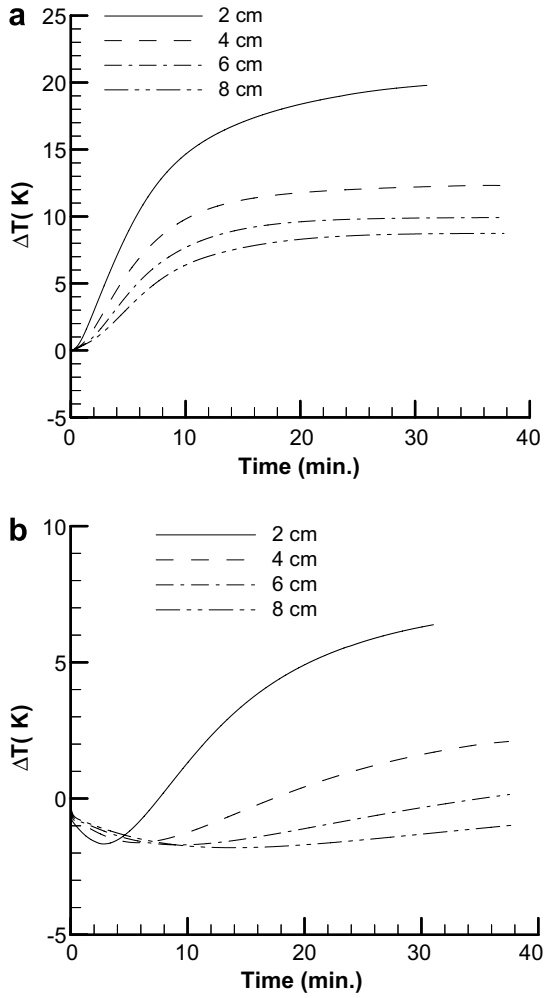

Fig. 5. The temperature rise at the (a) cathode catalyst layer and at the (b) surface of the methanol distribution layer during cell start-up.

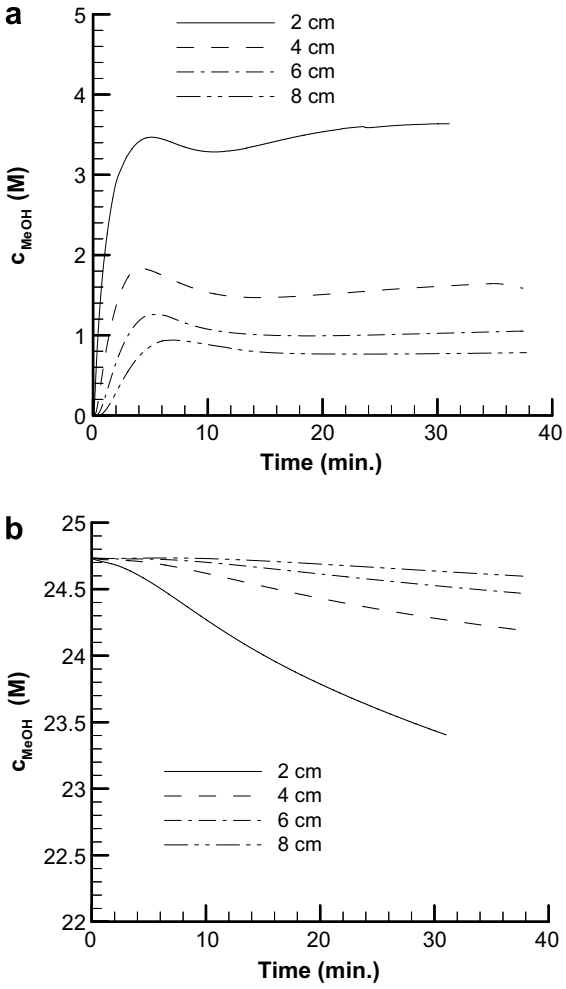

Fig. 6. Methanol feed concentration at (a) the surface of the anode gas diffusion layer and at (b) the end of the methanol distribution layer during start-up.

heat conduction rate through the gas is greater because the length is shorter. Also, for the shorter length scale, the fuel cell temperature reaches a higher value. Therefore, the methanol distribution layer's temperature increases for the shorter length scales, but remains under the initial temperature for the longer length scales for the duration of the simulations.

The methanol concentrations at the surface of the anode gas diffusion layer and at the end of the methanol distribution layer are presented in Fig. 6. The methanol concentration at the surface of the anode gas diffusion layer increases rapidly to a relative maximum value, then decreases. The methanol concentration starts to decrease for two reasons: first as the cell temperature rises, the reaction rate increases, and more methanol is consumed. Second, as the cell temperature rises, the partial pressure of methanol also rises, therefore, the driving force of the methanol transport across the vapor diffusion region is decreased. At the surface of the methanol distribution region, the methanol concentration decreases because water from the fuel cell condenses on this surface. Since the binary diffusion coefficient of a methanol/water solution is small, the water that condenses on this surface cannot diffuse through the methanol at a fast enough rate, therefore the water concentration accumulates at the surface. This phenomenon also reduces the driving force of methanol vapor in the vapor diffusion region and can potentially lead to a reduction in cell performance.

The usage ratio, η, is defined as the amount of a component used, over the amount produced or consumed of that same component in the chemical reactions.

$$\eta_{\text{Current}} = \frac{\mathbf{I}}{(\mathbf{I}+\mathbf{I}_c)}; \quad \eta_{\text{MeOH,evap}} = \frac{6F\int \dot{m}'''_{\text{MeOH,lv}}\mathrm{d}V}{M(\mathbf{I}+\mathbf{I}_c)A_{\text{cell}}}; \quad \eta_{\text{H}_2\text{O}} = \frac{3F\int \dot{m}'''_{\text{H}_2\text{O,lv}}\mathrm{d}V}{M(\mathbf{I}+\mathbf{I}_c)A_{\text{cell}}} \tag{48}$$

The water usage, comparing the water produced in the chemical reaction to the water evaporated is presented in Fig. 7. The water usage is always less than one, therefore the methanol concentration of the fuel cell will dilute and the cell power will decrease until the water usage ratio ap-

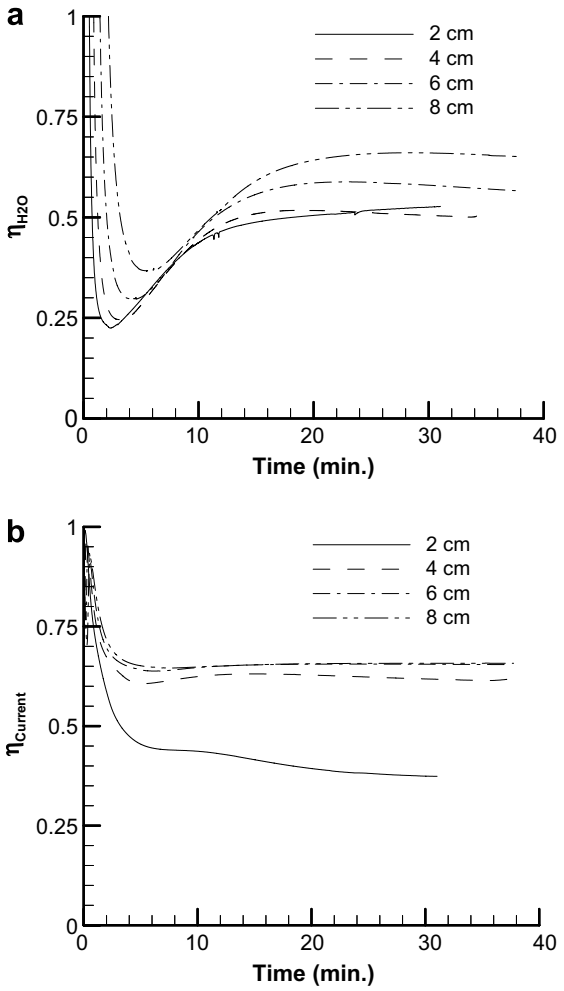

Fig. 7. Usage ratio for (a) water evaporation (b) useful current and start-up for different vapor diffusion region lengths.

proaches unity. With low water usage ratios there is an increased risk of flooding, since not enough water is leaving the system. The fuel usage of methanol to produce useful current compared to the total amount of methanol used is also presented in Fig. 7. This fuel usage is much less for the shorter vapor diffusion lengths, because the methanol concentration in the fuel cell is much greater, therefore there is much more methanol cross-over. However, as the vapor diffusion length increases, the methanol usage ratios begin to lie on top of each other.

5. Conclusions

The fundamentals of passive vapor fuel delivery to a direct methanol fuel cell are examined. The water management in a passive vapor fuel delivery system is crucial in the fuel cell as well as in the methanol distribution layer. The net water produced was found to be greater than the water evaporated for several different vapor diffusion lengths. Also, the back-diffusion of water to the methanol distribution layer was found to be a crucial issue for extended operation since the water that condenses can limit the methanol transport.

References

[1] Z. Guo, A. Faghri, Minature DMFCs with passive thermal-fluids management system, J. Power Sources 160 (2006) 1142–1155.
[2] Z. Guo, A. Faghri, Thermal-fluids management system for direct methanol fuel cells, Pending United States Patent 20060292412, 2006.
[3] Z. Guo, A. Faghri, Development of planar air breathing direct methanol fuel cell stacks, J. Power Sources 160 (2006) 1183–1194.
[4] Z. Guo, A. Faghri, Plannar fuel cell stack and method of fabrication of the same, Pending United States Patent 20060286436, 2006.
[5] G. Jewett, Z. Guo, A. Faghri, Water and air management systems for a passive direct methanol fuel cell, J. Power Sources 168 (2007) 434–446.
[6] Z. Guo, A. Faghri, Vapor feed direct methanol fuel cells with passive thermal-fluids management system, J. Power Sources 167 (2007) 378–390.
[7] Z. Guo, A. Faghri, Vapor feed fuel cells with a passive thermal-fluids management system, Pending United States Patent, 2005.
[8] H. Kim, Passive direct methanol fuel cells fed with methanol vapor, J. Power Sources 162 (2006) 1232–1235.
[9] H. Kim, J.M. Oh, J.Y. Lee, H. Chang, Fuel cell system comprising vapor-phase fuel supplying system, United States Patent 20060269825, 2006.
[10] H. Fukunaga, T. Ishida, N. Teranishi, C. Arai, K. Yamada, Impedance of vapor feed direct methanol fuel cells-polarization dependence of elementary processes at the anode, Electrochim. Acta 49 (2004) 2123–2129.
[11] A.K. Shukla, P.A. Christensen, A. Hamnett, M.P. Hogarth, A vapor-feed direct-methanol fuel cell with proton-exchange membrane electrolyte, J. Power Sources 55 (1995) 87–91.
[12] M. Hogarth, P. Christensen, A. Hamnett, A. Shukla, The design construction of high-performance direct methanol fuel cells. 2. Vapor-feed systems, J. Power Sources 69 (1997) 125–136.
[13] K. Scott, W. Taama, J. Cruickshank, Performance and modeling of a direct methanol solid polymer electrolyte fuel cell, J. Power Sources 65 (1997) 159–171.
[14] H. Dohle, J. Divisek, R. Jung, Process engineering of the direct methanol fuel cell, J. Power Sources 86 (1–2) (2000) 469–477.
[15]] A.A. Kulikovsky, J. Dvisek, A.A. Kornyshev, Two-dimensional simulation of direct methanol fuel, cell: a new (embedded) type of current collector, J. Electrochem. Soc. 147 (3) (2000) 952–959.
[16] C.Y. Wang, Fundamental models for fuel cell engineering, Chem. Rev. 104 (2004) 4727–4765.
[17] A. Faghri, Z. Guo, Challenges and opportunities of thermal management issues related to fuel cell technology and modeling, Int. J. Heat Mass Transfer 48 (2005) 3891–3920.
[18] J. Rice, A. Faghri, A transient, multi-phase and multi-component model of a new passive DMFC, Int. J. Heat Mass Transfer 49 (2006) 4804–4820.
[19] J. Rice, A. Faghri, Thermal and start-up characteristics of a miniature passive liquid feed DMFC system, including continuous/discontinuous phase limitations, ASME J. Heat Transfer, in press.
[20] A. Faghri, Y. Zhang, Transport Phenomena in Multiphase Systems, Elsevier Inc., 2006.
[21] D.R. Lide (Ed.), Handbook of Chemistry and Physics, Eigthy fifth Ed., CRC Press, USA, 2004.
[22] C.L. Yaws, Handbook of Transport Property Data: Viscosity, Thermal Conductivity and Diffusion Coefficients of Liquid and Gases, Gulf Pub. Co., Houston, TX, 1995.
[23] C.L. Yaws, Thermodynamics and Physical Property Data, Gulf Pub. Co., Houston, TX, 1992.
[24] A. Faghri, Heat Pipe Science and Technology, Taylor & Francis, USA, 1995.

[25] X. Ren, T.E. Springer, A. Zawodzinski, S. Gottesfeld, Methanol transport through nafion membranes, electro-osmotic drag effects on potential step measurements, J. Electrochem. Soc. 147 (2) (2000) 466–474.
[26] Z.H. Wang, C.W. Wang, Mathematical modeling of liquid-feed direct methanol fuel cells, J. Electrochem. Soc. 150 (4) (2003) A508–A519.
[27] J.P. Meyers, J. Newman, Simulation of the direct methanol fuel cell, J. Electrochem. Soc. 149 (6) (2002) A718–A728.